OPEN ACCESS

Passivity-Constrained Hybrid Learning for Two-Phase Flow Networks: Port-Hamiltonian Modeling and Risk-Sensitive State Estimation

Rizky Pratama,[1] Arif Nugroho[2]

[1] Universitas Jenderal Soedirman, Jalan Profesor Dr. HR Boenyamin No. 708, Grendeng, Purwokerto, Jawa Tengah, Indonesia;
[2] Universitas Trunojoyo Madura, Jalan Raya Telang PO Box 2, Kamal, Bangkalan, Jawa Timur, Indonesia;

Abstract

Gas–liquid two-phase flow is a recurring challenge in energy and process systems because the macroscopic variables that operators measure and control are shaped by strongly nonlinear interfacial dynamics. In field practice, sparse telemetry and uncertain closures make it difficult to maintain stable pressure and flow delivery when operating conditions change rapidly. This paper develops a digital-twin methodology that is explicitly designed for online decision support in two-phase flow networks, emphasizing stability guarantees rather than solely predictive accuracy. The main contribution is a passivity-constrained hybrid model that combines a port-Hamiltonian network representation of two-phase transport with learned dissipative and interfacial closure terms. The network model exposes power ports at boundaries and junctions, enabling a consistent treatment of pumps, chokes, compressors, and valves as energy-shaping elements. Learning is restricted by inequality constraints that preserve passivity and prevent nonphysical energy generation, which is critical for robust rollout during transients. To assimilate telemetry, we derive a risk-sensitive smoothing formulation that jointly estimates hidden states and closure multipliers while penalizing underestimation of tail risk in pressure and holdup. The resulting estimator outputs calibrated predictive bands that can be propagated through a safety-aware controller. A constrained receding-horizon policy uses the twin to enforce probabilistic pressure and flow limits under regime ambiguity and sensor bias. Computational experiments demonstrate improved stability under aggressive actuation and improved reliability under sensor dropout compared to unconstrained learning baselines, while maintaining competitive point-forecast error.

1. Introduction

Two-phase transport of gas and liquid through wells, risers, pipelines, and surface facilities exhibits a peculiar combination of physical structure and operational fragility [1]. The underlying governing laws are conservation of mass and momentum, but the practical predictions hinge on closure relations for slip, friction, interfacial shear, compressibility effects, and phase distribution. These closures are sensitive to geometry, inclination, roughness, and transient history, and they often change qualitatively when the internal flow structure reorganizes. Operators therefore face a dual problem: they must infer an evolving internal state from limited sensors, and they must choose control actions that keep the system within safe constraints even when the effective dynamics shift.

Historically, many operational models are built around averaged one-dimensional equations with empirical closure functions. These models are valuable because they encode invariants and enable physically meaningful extrapolation, yet their reliability degrades when deployed outside calibration envelopes or when the system is driven through rapid transients. At the same time, purely data-driven predictors can fit complicated mappings from measured inputs to outputs but may violate conservation structure, become unstable in closed-loop operation, and provide limited assurances under distribution shift [2]. A digital twin that is intended to participate in real-time decision support must therefore reconcile three goals that are often treated separately: physical consistency, learnable adaptability, and stability under control.

This paper adopts an energy-based viewpoint to reconcile these goals. Instead of beginning with a discretization of two-fluid equations and then adding learned correction terms, we begin with a port-Hamiltonian representation of a two-phase network. In that representation, the

Copyright by the Authors.
Licensed as an open access article using a CC BY 4.0 license.

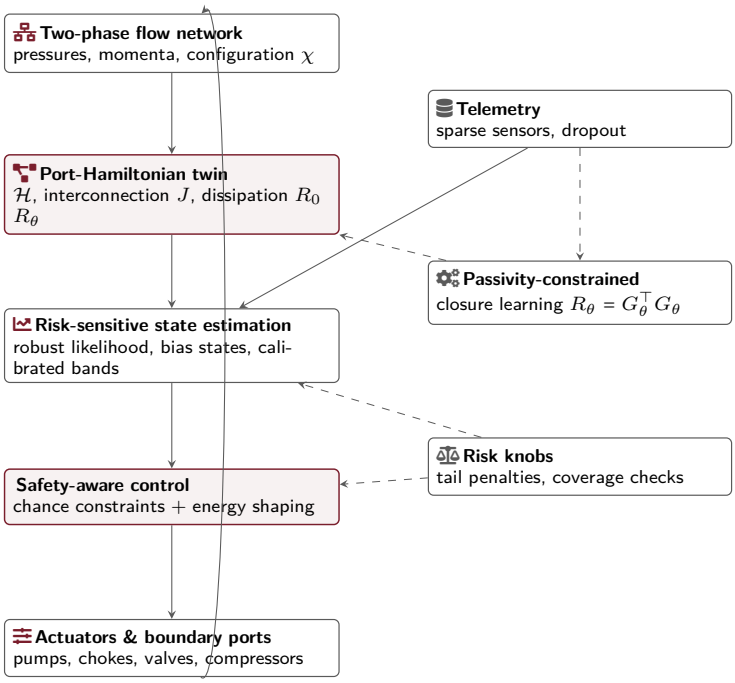


Figure 1: Stability-first digital-twin loop: a port-Hamiltonian network model with passivity-preserving learned dissipation supports risk-sensitive state estimation and a safety-aware controller that acts through boundary power ports.

system is defined by a stored-energy functional, an interconnection structure that preserves power balance, and dissipation terms that remove energy. The physical meaning is that pumps and boundary conditions exchange power through ports, while friction and interfacial interactions dissipate power. The key benefit is that stability properties can be expressed as passivity inequalities, which remain meaningful when the model is coupled to controllers and estimators [3].

Passivity is not a decorative property in this setting. Many operational instabilities that arise in two-phase flow management are manifestations of unmodeled energy injection, numerical artifacts, or closure terms that inadvertently produce negative damping. When learned surrogates are inserted into mechanistic models without constraints, they can create precisely such artifacts, leading to oscillations or runaway pressure predictions during rollout. A passivity-constrained learning strategy provides a principled method to prevent this class of failure, even when the learned components are flexible function approximators. The thesis of the paper is that a stability-first digital twin can be built by learning only those closure components that are provably dissipative and by embedding them in a network model that enforces power balance at interconnections.

The approach is compatible with, but not defined by, discriminative regime identification efforts [4]. For example, Manikonda et al. (2021) reported what were first-of-a-kind and then state-of-the-art machine learning classification models that accurately predicted gas–liquid two-phase flow regimes in annular flow channels [5], illustrating that data-driven methods can capture regime information from measured features [5]. In the present work, regime information is treated as a latent contributor to dissipation and slip variability rather than as the primary output. The goal is not to produce a regime map, but to build a dynamical twin that remains stable, calibrates uncertainty, and supports safe actuation despite regime ambiguity.

The remainder of the paper is organized around the components needed for this stability-first twin. We first derive an energy-consistent network model for two-phase transport that exposes ports and junction constraints in a way that is natural for control [6]. We then introduce a constrained learning formulation that parameterizes uncertain dissipation and interfacial terms while enforcing passivity inequalities across operating conditions. Next, we develop a risk-sensitive state estimation method that as-

Symbol	Description	Role in digital twin
x	Aggregate network state (pressures, momenta, configurations)	Encodes internal dynamics of the two-phase network
u	Port input vector (pump heads, choke drops, valve coefficients)	Represents externally applied power and actuation
y	Port output vector (pressures, flows at ports)	Provides measured and virtual outputs for estimation and control
$\mathcal{H}x$	Stored-energy functional	Certifies passivity and defines the energy landscape for stability
Jx	Skew-symmetric interconnection matrix	Enforces power-conserving coupling across edges and junctions
Rx	Symmetric positive semidefinite dissipation mapping	Encodes wall friction, interfacial drag, and configuration relaxation

Table 1: Key variables and operators in the port-Hamiltonian representation of gas–liquid two-phase flow networks.

Layer	Description	Main design choices
Port-Hamiltonian core	Energy-consistent network model on a directed graph	Semi-discretized edges, incidence-based Jx, convex storage $\mathcal{H}x$
Passivity-constrained learning	Data-driven corrections to dissipation and interfacial terms	Factorized $R_\theta x = G_\theta^\top G_\theta$, physically motivated features
Risk-sensitive estimation	Robust smoother with closure adaptation and bias states	Heavy-tailed likelihood, risk functional on safety-critical pressures
Safety-aware control	Receding-horizon optimization with probabilistic constraints	Chance constraints, scenario sampling, energy-based tightening
Configuration surrogate	Continuous state capturing regime-dependent behavior	Multistable potential in $\mathcal{H}$ and dissipation dependence on χ

Table 2: Main architectural layers of the stability-focused two-phase flow digital twin.

similates sparse telemetry and produces predictive distributions tuned for tail-risk management. We then integrate these elements into a safety-aware control layer that uses the twin to enforce probabilistic constraints on pressure and flow. Finally, we evaluate the framework on computational scenarios designed to stress stability under aggressive actuation, sensor dropout, and distribution shift, and we discuss practical deployment considerations such as computational cost and online adaptation.

2. Port-Hamiltonian Network Model of Gas--Liquid Two-Phase Transport

A network representation is essential in operational settings because wells, manifolds, risers, pipelines, and separators form interconnected systems with junctions, boundary ports, and actuators. We model the system as a directed graph with edges representing conduit segments and nodes representing junctions, sources, sinks, or control devices [7]. Each edge carries a reduced two-phase state that evolves in time, and each node imposes algebraic constraints that enforce continuity of pressure or conservation of mixture flow. The objective of this section is not to reproduce a detailed multiphase PDE model, but to define a structured dynamical system whose stability properties can be stated in terms of stored energy and dissipation.

Let x denote the collection of edge states, aggregated over the network. For each edge, we define a state vector that includes a compressible pressure-like variable and a momentum-like variable, as well as an internal configuration variable that reflects phase distribution. The configuration variable is not assumed to be a direct regime label; instead, it serves as a continuous surrogate for slip and holdup variability. The edge dynamics are coupled through nodal constraints that tie together boundary pressures and mixture fluxes [8]. External controls act through boundary ports, such as pump heads, choke pressure drops, or valve coefficients. Measurements include pressures at selected nodes, mixture flow at selected edges, and possibly indirect signals correlated with holdup.

Element	State / variables	Constraints and interfaces
Edge segment	Local pressure, momentum, configuration surrogate	Semi-discrete dynamics with compressibility and slip-dependent kinetics
Junction node	Nodal pressure and incident edge flows	Mixture flow conservation and pressure continuity up to actuator drops
Boundary port	Boundary pressure, flow, or head	Power exchange between network and environment or equipment
Actuator	Pump speed, choke opening, valve position	Modeled as energy-shaping and dissipative elements at ports
Sensor	Pressure, flow, or proxy holdup measurement	Provides partial observations with possible bias and heavy-tailed noise

Table 3: Network elements, associated variables, and interconnection constraints in the port-Hamiltonian model.

Term	Mathematical structure	Physical interpretation
$\mathcal{H}x$	Sum of local storage terms over edges and volumes	Total mechanical energy stored in compressibility and momentum
$\mathcal{H}_p p_{e,i}$	Convex function of pressure-like variable	Compressible storage for two-phase mixture in a control volume
$\mathcal{H}_m m_{e,i}, \chi_{e,i}$	Convex kinetic term depending on configuration	Kinetic energy with effective density and slip dependence
Configuration potential	Multistable potential over $\chi_{e,i}$	Encodes hysteresis and regime-like transitions in internal structure
Edge-wise sum	$\mathcal{H} = {}_{e\ i}\mathcal{H}_p\ \ \mathcal{H}_m$	Aggregation that preserves convexity and supports sparse gradients

Table 4: Decomposition of the Hamiltonian into compressible storage, kinetic energy, and configuration-dependent components.

In a port-Hamiltonian formulation, the evolution is expressed through an interconnection matrix and a dissipation mapping. The Hamiltonian $\mathcal{H}x$ represents stored energy, which in a compressible conduit segment includes fluid compressibility and kinetic energy contributions. The system is driven by port variables u, y that satisfy a power identity, and internal dissipation removes energy. A generic port-Hamiltonian form for the network is

$$x = \big(Jx - Rx\big)\,\nabla\mathcal{H}x \qquad Bx\,u \tag{2.1}$$

where Jx is skew-symmetric and encodes the power-conserving interconnection structure, Rx is symmetric positive semidefinite and encodes dissipation, and Bx maps external ports to the internal states [9]. The measured port output is defined as

$$y = Bx^{\top}\nabla\mathcal{H}x. \tag{2.2}$$

The key stability property is obtained by differentiating $\mathcal{H}$ along trajectories. Using skew-symmetry of J, one obtains

$$\mathcal{H}x = -\nabla\mathcal{H}x^{\top}Rx\,\nabla\mathcal{H}x \qquad u^{\top}y, \tag{2.3}$$

which shows that, in the absence of input power, the stored energy cannot increase. This inequality formalizes passivity, and it remains valid under interconnection of passive subsystems. For two-phase networks, this is significant because it provides a modular stability logic: if each edge model is passive and each actuator model is passive, then the full interconnection is passive.

The challenge is that two-phase closures appear inside Rx and sometimes inside the definition of $\mathcal{H}x$ through effective density and compressibility. Traditional closures may not be easily expressed in a guaranteed-dissipative form, especially when they depend on unobserved phase distribution variables [10]. Moreover, in operational practice, one often introduces empirical correction factors that can inadvertently break passivity. The approach in this paper is to parameterize uncertain terms directly within the dissipation mapping and to constrain them to remain

Component	Nominal part $R_0 x$	Learned correction $R_\theta x$	Passivity enforcement
Wall friction	Mechanistic closure with geometry-based friction factors	Data-driven multipliers modulating friction intensity	Factorization $R_\theta = G_\theta^\top G_\theta$
Interfacial drag	Empirical slip and shear relations	State- and χ-dependent correction to coupling terms	Restriction to nonnegative dissipation channels
Configuration relaxation	Baseline relaxation rate in configuration dynamics	Learned dependence of relaxation on flow conditions	Gradient-like dynamics tied to configuration potential
Cross-coupling	Sparse nominal coupling between momentum states	Low-rank learned coupling aligned with topology	Structured basis limiting degrees of freedom
Global regularization	None in purely mechanistic model	Smoothness and Lipschitz penalties on G_θ	Prevents sharp local energy removal or injection

Table 5: Structure of dissipation and interfacial closure modeling, combining nominal physics and passivity-constrained learning.

Aspect	Modeling choice	Purpose in estimation	Additional notes
Process model	Discrete-time port-Hamiltonian dynamics $x_{k1} = f x_k, u_k, \theta_k \; w_k$	Propagate hidden pressures, momenta, and configurations	Exploits sparsity and passivity for numerical robustness
Measurement model	$y_k = h x_k \; b_k \; v_k$ with partial and indirect sensors	Fuse telemetry with model predictions	Allows bias separation from true state evolution
Bias evolution	Random-walk bias b_k with occasional jumps	Capture sensor drift and recalibration events	Prevents overfitting model to faulty measurements
Risk functional	Convex penalty on near-limit pressures and flows	Emphasize tail risk in safety-critical quantities	Influences posterior variance inflation near constraints
Robust penalties	Heavy-tailed or Huberized residuals ρ_w, ρ_v	Downweight outliers and transient spikes	Supports calibrated intervals during aggressive transients
Implementation	Iterated Gauss–Newton smoother with sparse linear algebra	Scalable inference on large networks	Produces predictive bands for controller use

Table 6: Design elements of the risk-sensitive state estimator applied to the port-Hamiltonian two-phase network model.

positive semidefinite. In doing so, we preserve the energy inequality even after learning and adaptation.

To connect the abstract representation to a computational model, we consider a semi-discretization of each edge into a small number of control volumes. Within each volume, the pressure-like variable represents compressible storage, while the momentum-like variable represents a mixture momentum that accounts for slip indirectly. The Hamiltonian is chosen as a sum of convex storage terms: [11]

$$\mathcal{H}x = \sum_{e\,i} \big(\mathcal{H}_p p_{e,i} \; \mathcal{H}_m m_{e,i}, \chi_{e,i}\big), \tag{2.4}$$

where $p_{e,i}$ is the pressure-like component, $m_{e,i}$ is the momentum-like component, and $\chi_{e,i}$ is the configuration surrogate. The storage term $\mathcal{H}_p$ is selected to reflect compressibility and to ensure convexity over the operational pressure range. The term $\mathcal{H}_m$ reflects kinetic energy and can depend on χ because effective density and slip affect the mapping from momentum to velocity. The convexity of $\mathcal{H}$ is important because it supports well-posedness of the gradient mapping and facilitates estimation.

Interconnections at nodes are handled by algebraic constraints that enforce conservation of mixture flow and continuity of pressure up to actuator-induced drops. These constraints can be encoded in the interconnection matrix Jx, which is built from incidence matrices of the graph.

Element	Definition	Role in control layer	Notes
Stage cost	$\ell x_t, u_t$ combining tracking and actuation penalties	Balance production objectives with effort and risk	Includes penalties on input power to discourage aggressive actions
Chance constraint	$\Pr g x_t, u_t \leq 0 \geq 1 - \delta$	Limit probability of pressure and flow violations	Uses predictive distributions from the estimator
Prediction horizon	Length N receding-horizon window	Capture compressibility-driven transients	Tuned to actuation and wave-propagation time scales
Scenario sampling	Trajectories under sampled states and disturbances	Approximate chance constraints under nonlinear dynamics	Incorporates uncertainty in closure multipliers and biases
Energy-based tightening	Bounds derived from $\mathcal{H} \leq u^\top y$	Prune unsafe control sequences and certify safety	Uses passivity to constrain reachable pressure excursions

Table 7: Main ingredients of the safety-aware receding-horizon controller interfaced with the digital twin.

Configuration	Model structure	Learning / estimation treatment	Control strategy
Mechanistic baseline	Fixed nominal port-Hamiltonian network	No learned dissipation; static closures	Deterministic receding-horizon with point forecasts
Unconstrained learned	Nominal model plus free learned corrections	Flexible closures without passivity guarantees	Optimization on potentially non-passive dynamics
Passive learned only	Passivity-constrained dissipation corrections	Offline training with structural regularization	Deterministic control using stabilized twin
Full framework	Passivity-constrained twin with risk-sensitive estimation	Online closure adaptation with bias and uncertainty	Chance-constrained controller using predictive bands

Table 8: Model-controller combinations compared in the computational evaluation of stability and reliability.

One benefit of an incidence-based construction is that skew-symmetry can be ensured by design, preventing numerical artifacts from creating artificial energy sources. The result is a network model that is structurally stable before any learning is introduced.

However, the model is not complete without specifying how two-phase effects influence dissipation and coupling. In this work, we treat wall friction and interfacial exchange as dissipative terms and encode them in Rx. For example, a frictional pressure drop contributes a dissipation proportional to the square of a generalized flow variable, and interfacial drag contributes a dissipation proportional to the square of a slip-related variable [12]. The unknown part is the coefficient function that maps state and configuration to dissipation magnitude. This coefficient is where learning enters, but learning is restricted to preserve positive semidefiniteness of Rx, ensuring that the energy inequality holds regardless of the learned parameter values.

A final modeling point is that two-phase systems can exhibit regime-dependent behavior that is not fully captured by smooth changes in χ. We represent this by allowing χ to evolve under a bistable or multistable potential within the Hamiltonian and by allowing the dissipation coefficients to depend on χ in a nonlinear way. This captures hysteresis and delayed transitions without forcing the model to switch discretely between regimes. The resulting model supports both smooth adaptation and abrupt qualitative changes, while remaining within the passivity envelope [13].

3. Passivity-Constrained Learning of Dissipation and Interfacial Closures

Learning enters the digital twin through uncertain dissipative and interfacial closure terms. The guiding princi-

Scenario family	Perturbation type	Primary evaluation metrics
Aggressive actuation	Rapid setpoint changes in downstream pressure and actuator limits	Pressure tracking error, transient stability, magnitude of oscillations
Sensor dropout	Intermittent loss of pressure and flow measurements	Constraint violation frequency, uncertainty inflation, control aggressiveness
Distribution shift	Changes in roughness and geometry affecting effective friction	Bias in pressure predictions, adaptability of dissipation multipliers
Configuration ambiguity	Inputs that drive rapid changes in internal structure	Coverage of predictive intervals, smoothness of control actions
Classifier-assisted baseline	Regime probabilities modulating dissipation	Impact of discontinuous closures on stability and tracking performance

Table 9: Computational scenario families used to assess stability, robustness to telemetry issues, and performance under distribution shift.

ple is that the learned components must not create net energy, because doing so can destabilize closed-loop operation and can cause nonphysical predictions during rollout. This section defines a parameterization for the uncertain terms and a training objective that enforces passivity as a hard constraint, while still allowing sufficient flexibility to fit operational data.

We write the dissipation matrix as a sum of a nominal component and a learned component:

$$Rx = R_0 x \;\; R_\theta x, \tag{3.1}$$

where R_0 encodes baseline friction and drag derived from mechanistic reasoning, and R_θ is a learned correction that accounts for geometry uncertainty, unmodeled slip effects, and regime-dependent changes. Passivity requires $Rx \succeq 0$ for all relevant x, so we impose $R_\theta x \succeq -R_0 x$, and in practice we enforce $R_\theta x \succeq 0$ to preserve interpretability as an additional dissipation [14]. This restriction is not overly conservative because many practical mismatches manifest as underestimation of dissipation or as misallocation of dissipation across components.

To ensure positive semidefiniteness, we parameterize $R_\theta x$ through a factorization:

$$R_\theta x = G_\theta x^\top G_\theta x, \tag{3.2}$$

where $G_\theta x$ is a learned matrix-valued function. This construction guarantees $R_\theta x \succeq 0$ for any θ. The function G_θ can be implemented as a neural network or as a kernel regression model, but it is restricted to depend on a set of physically meaningful features, such as pressure, mixture velocity, and configuration χ, rather than on arbitrary embeddings. This feature restriction improves sample efficiency and reduces the risk of spurious dependence on noise [15].

Interfacial and slip effects are treated similarly. Rather than learning a direct mapping from state to holdup, we learn coefficients that modulate dissipative coupling between momentum and configuration states. The configuration dynamics are chosen to be gradient-like with respect to a potential in the Hamiltonian, which ensures that, absent input power, configuration changes do not increase stored energy. The learned terms then influence the rate at which configuration relaxes and the degree to which configuration couples into momentum dissipation. This approach avoids representing regime changes as unconstrained discrete jumps, which can break passivity unless carefully handled.

Training is performed by matching measured outputs and by minimizing residuals of the network dynamics [16]. Let $\{ut, yt\}$ denote input-output data collected from simulations, experiments, or operations over time intervals. The model predicts $\hat{y}t; \theta$ by integrating the port-Hamiltonian system with the learned dissipation. The basic data-fit objective is a least-squares term weighted by measurement covariance. To reduce drift and enforce dynamic consistency, we add a penalty on the mismatch between predicted and filtered state derivatives when a rough derivative estimate is available. The training problem is then

$$\min_{\theta} \quad \|yt - \hat{y}t; \theta\|_W^2 \, dt \\ \lambda \, \|\hat{x}t; \theta - \tilde{f}t\|^2 \, dt \tag{3.3}$$

subject to the structural constraint $R_\theta x = G_\theta x^\top G_\theta x$. Here W is a weighting matrix and $\tilde{f}t$ is an auxiliary esti-

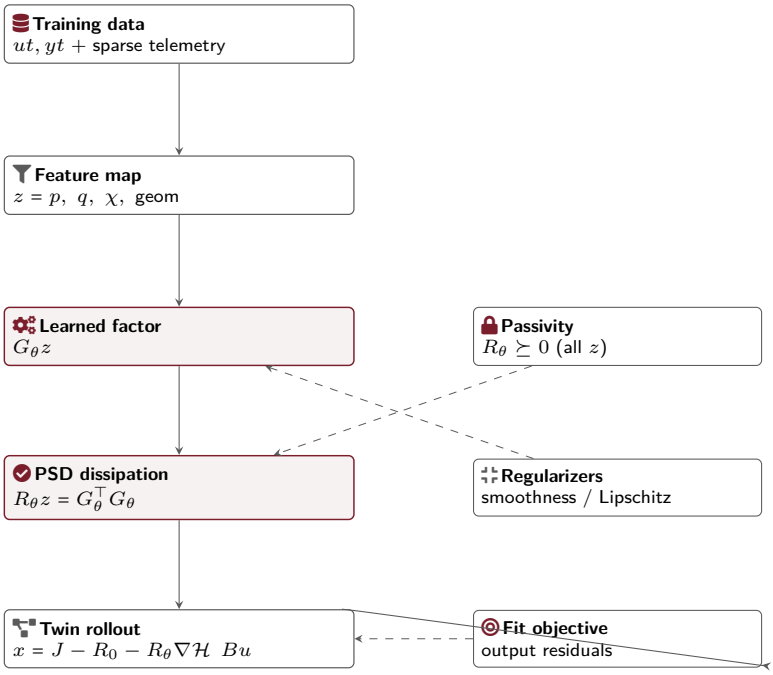


Figure 2: Passivity-constrained closure learning: uncertain friction/interfacial terms are parameterized through a learned factor G_θ so that $R_\theta = G_\theta^\top G_\theta$ remains positive semidefinite, preventing spurious energy injection during rollout and control embedding.

mate of state evolution derived from a smoother or from finite differences when available.

A central concern is overfitting, especially because operational datasets can be biased by limited exploration of the input space. Passivity reduces one class of overfitting by disallowing energy-injecting artifacts, but additional regularization is needed to avoid overly complex dissipation landscapes that interpolate noise [17]. We incorporate a Lipschitz penalty on G_θ over the relevant feature domain and a smoothness penalty that discourages sharp variations in dissipation with respect to pressure and flow. These penalties are consistent with the physical intuition that friction and interfacial drag vary smoothly with operating conditions, except near strong transitions that are captured through the configuration variable dynamics.

The learning problem is further complicated by partial observability. In many networks, only a subset of node pressures and edge flows are measured, and holdup-related variables are rarely observed directly. Learning dissipation purely from output error can be ill-posed because multiple internal dissipation distributions can explain the same boundary measurements. We address this by incorporating structural identifiability cues [18]. In particular, we choose a low-dimensional basis for dissipation corrections aligned with the network topology, such as per-edge scalar multipliers on nominal friction terms and a small number of coupling coefficients that represent interfacial exchange intensity. The learned function G_θ then maps features to these multipliers rather than to a fully dense matrix. This provides a compromise: the model can adapt across operating conditions, but it does so through a parsimonious set of physically interpretable degrees of freedom.

Even with a parsimonious basis, regime-dependent behavior can lead to multimodal posterior distributions over dissipation parameters. If the system can occupy different internal configurations that yield different effective friction, then an estimator may be uncertain about which configuration is present. The learning method must therefore accommodate data that reflect multiple modes [19]. We handle this by training on ensembles of trajectories that cover different transient histories, and by including the configuration surrogate as a state that evolves according to the model. In effect, the model internalizes some regime variability as a dynamical state rather than forcing it into static parameter values.

Finally, the passivity constraint provides a clean interface to safe control. Because learned dissipation cannot generate energy, a controller that shapes input power can rely on the digital twin to remain stable under rollout. This is essential when the twin is used inside an optimizer that evaluates many candidate control sequences. Without

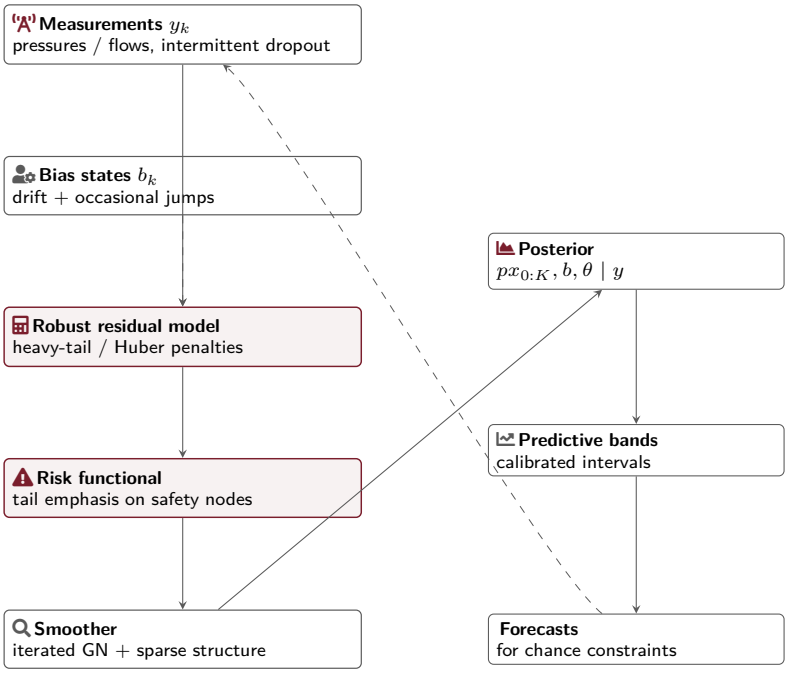


Figure 3: Risk-sensitive estimation pipeline: robust penalties and explicit tail-risk shaping produce posterior distributions and predictive bands that remain cautious during transients, sensor bias, and telemetry dropout.

such a constraint, the optimizer can exploit model artifacts and propose actions that appear safe in the model but are unsafe in reality [20]. Passivity reduces this exploitability by eliminating a broad family of unphysical behaviors.

4. Risk-Sensitive State Estimation with Closure Adaptation

A model is operationally useful only if it can track the internal state online from limited measurements. Two-phase networks present a difficult inference problem because internal variables such as configuration and holdup are weakly observed, sensors can be biased, and measurement noise can be heavy-tailed during transients. Moreover, if the twin is used for safety management, it must avoid underestimating tail risk in pressure and flow. This section derives a risk-sensitive estimator designed for these conditions, emphasizing calibrated predictive uncertainty and robust handling of outliers.

We write a discrete-time approximation of the network dynamics for estimation: [21]

$$\begin{aligned} x_{k1} &= f x_k, u_k, \theta_k \;\; w_k \\ y_k &= h x_k \;\; b_k \;\; v_k, \end{aligned} \tag{4.1}$$

where x_k includes pressures, momenta, and configurations across the network, θ_k are slowly varying closure multipliers produced by the passivity-constrained learning parameterization, b_k are sensor biases, and w_k, v_k are process and measurement disturbances. The disturbances are not assumed Gaussian; instead, we use a robust likelihood model that downweights outliers. A practical choice is a Student-like likelihood or a Huberized quadratic, implemented through an equivalent latent-scale representation to preserve computational tractability.

Risk sensitivity is introduced by modifying the objective of the smoother. Instead of minimizing expected squared error, we minimize an exponential-of-quadratic criterion that penalizes large deviations more heavily. In a filtering context, this is related to risk-sensitive control and robust estimation. A convenient formulation defines the estimator as the minimizer of [22]

$$\begin{aligned} \min_{x_{0:K}, b_{0:K}, \theta_{0:K}} \quad & \sum_{k=0}^{K-1} \rho_w \Delta_k \\ & \sum_{k=0}^{K} \rho_v r_k \\ & \gamma \sum_{k=0}^{K} \Phi x_k, \end{aligned} \tag{4.2}$$

where $\Delta_k = x_{k1} - f x_k, u_k, \theta_k$ are process residuals, $r_k = y_k - h x_k - b_k$ are measurement residuals, ρ_w, ρ_v are robust

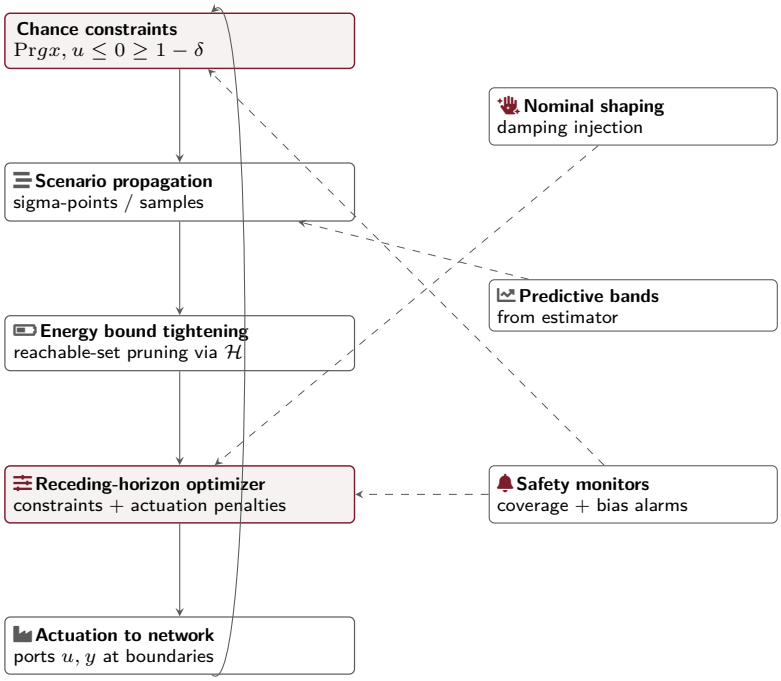


Figure 4: Safety-aware control stack: predictive uncertainty drives scenario-based chance constraints, while energy-based reachable-set tightening and nominal damping support reliable optimization under regime ambiguity and sensor bias.

penalties, and Φx_k is a risk functional that emphasizes tail behavior of safety-critical outputs such as pressure at specific nodes. The coefficient γ tunes the strength of risk sensitivity. The risk functional is chosen to be convex in the outputs of interest, for example a softplus approximation of an upper threshold exceedance penalty. The result is that the estimator favors trajectories that not only fit measurements but also avoid underestimating the probability of dangerous pressure excursions.

A core challenge is the interaction between state estimation and closure adaptation. If closure multipliers θ_k are allowed to vary freely, the estimator can attribute any mismatch to parameter drift, which can lead to overconfident state estimates and poor predictive generalization. We therefore enforce a slow-drift prior on θ_k and, crucially, we restrict θ_k to remain within the passivity-constrained family [23]. Practically, θ_k parameterizes the mapping $G_\theta x$ that yields additional dissipation, so θ_k cannot produce negative dissipation. We further penalize rapid changes in θ_k to reflect that physical properties such as roughness and effective drag do not change abruptly absent a regime transition. Regime-like shifts are instead captured through the configuration state χ, whose dynamics can change rapidly when driven by inputs.

We implement the estimator through an iterated Gauss–Newton procedure on the robust objective, combined with a square-root information filter for computational efficiency. The port-Hamiltonian structure assists computation because the Jacobians of f can be derived from the gradient of the Hamiltonian and the interconnection matrices, which are sparse due to network topology. Sparsity is critical for scalability because realistic networks can include dozens to hundreds of edges [24]. We exploit this sparsity by using sparse linear algebra in the smoother step and by maintaining local covariance approximations on subgraphs when full covariance propagation is too expensive.

Uncertainty quantification is produced through a Laplace approximation around the smoothing solution, yielding an approximate Gaussian posterior for the state and biases, and an approximate log-concave posterior for the closure multipliers when robust penalties are used. Because the measurement likelihood is heavy-tailed, the posterior variances increase during transients, which prevents spurious overconfidence. The risk functional further inflates uncertainty in safety-critical outputs when the state is weakly observed, aligning the estimator with operational needs. The twin therefore outputs not just point

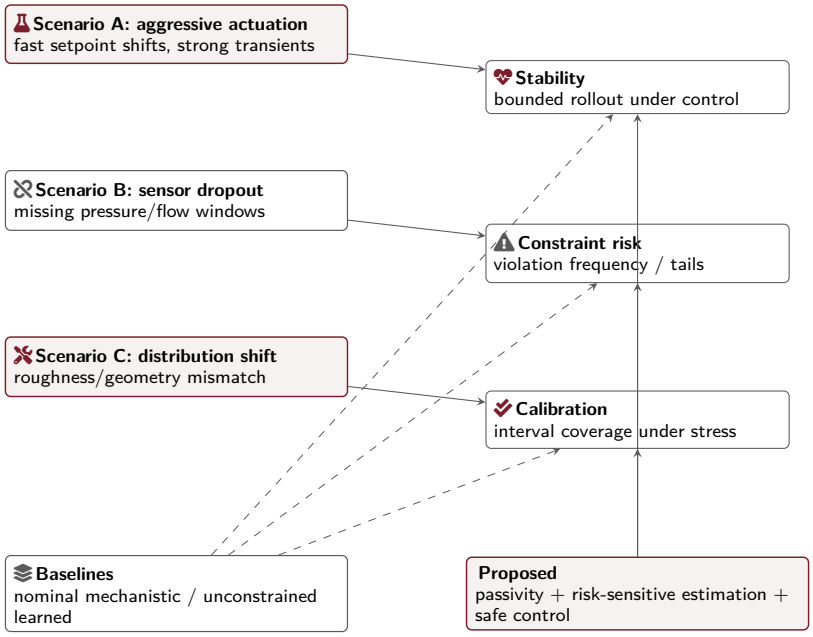


Figure 5: Stress-test evaluation design: three operating stresses (aggressive actuation, telemetry dropout, and parameter shift) are scored by stability, tail-risk of constraint violations, and predictive-interval calibration to highlight failure modes that average error can hide.

estimates of pressure but predictive bands that reflect both measurement uncertainty and model uncertainty in dissipation.

A practical complication is that sensor biases can confound the inference [25]. Pressure sensors can drift, flow meters can have scale errors, and some sensors can exhibit hysteresis. We model biases b_k as random walks with occasional jump components to reflect recalibration events or abrupt failures. The robust penalty on measurement residuals prevents a single bad sensor from forcing large changes in the inferred state. Additionally, because the network model enforces interconnection constraints, inconsistent sensor readings are naturally reconciled by distributing residuals across biases and unobserved states in a way that respects conservation structure.

The output of the estimator is a predictive distribution for future states under candidate control actions. To generate forecasts, we propagate the posterior mean through the port-Hamiltonian dynamics and propagate uncertainty through a sigma-point method adapted to the sparse structure [26]. The passivity constraint again plays a role: when uncertainty is large, naive propagation can produce implausible trajectories if the model admits energy injection. Because the learned dissipation is guaranteed nonnegative, the forecast remains stable, and uncertainty growth is dominated by process noise rather than by model-induced blow-up. This stability makes the twin usable inside online optimization loops for control.

5. Safety-Aware Control via Energy-Shaping and Chance Constraints

Control of two-phase flow networks is often framed as maintaining pressures within safety envelopes while meeting production or transport objectives. Actuators can include pump speeds, choke openings, compressor setpoints, and valve positions. In a network, local actions can have nonlocal effects due to compressibility and interconnection constraints [27]. A digital twin that is used for control must therefore provide reliable predictions under action-induced transients. This section develops a control interface that exploits the port-Hamiltonian structure and the risk-sensitive predictive distributions produced by the estimator.

We consider a receding-horizon control problem in which, at each time step, the controller selects a sequence of control inputs to minimize an objective subject to constraints. The objective penalizes deviation from desired pressures or flows and penalizes aggressive actuation. The constraints encode safety limits on pressures, limits on pump or choke operating ranges, and potentially

constraints on configuration variables that correlate with undesirable behaviors. Because the state estimate is uncertain, we enforce constraints probabilistically through chance constraints [28]. The control problem is

$$\begin{aligned} \min_{u_{k:kN-1}} \quad & \mathbb{E}\Big[\sum_{t=k}^{kN-1} \ell x_t, u_t\Big] \\ \text{s.t.} \quad & \Pr\big(g x_t, u_t \le 0\big) \ge 1-\delta \end{aligned} \tag{5.1}$$

for all t in the horizon, where δ is a risk tolerance. The expectation and probability are taken with respect to the predictive distribution generated by the twin.

Directly solving chance-constrained problems for nonlinear, uncertain dynamics can be computationally demanding. We adopt an approach that combines scenario sampling with energy-based constraint tightening. Scenario sampling draws multiple trajectories from the predictive distribution, including perturbations of initial state, process noise, and closure multipliers [29]. The constraints are enforced across the scenario set, either as hard constraints on all scenarios or as quantile constraints consistent with δ. Scenario-based methods are well-suited to multimodal uncertainty induced by configuration dynamics. However, they can still be expensive if many scenarios are needed for reliability.

Energy-based tightening provides an additional efficiency lever. Because the port-Hamiltonian model yields a stored-energy function $\mathcal{H}x$ and a dissipation inequality, we can derive bounds on how much certain outputs can change over the horizon under bounded input power. Specifically, if input power is bounded by actuator limits and if dissipation is nonnegative, then the growth of $\mathcal{H}$ is constrained, which implies constraints on the reachable set of pressures. While these bounds are conservative, they can be used to prune candidate control sequences early in optimization, reducing computational burden. They also provide a safety certificate: even if the uncertainty propagation is imperfect, the energy inequality limits the extent of unmodeled excursions under bounded actuation [30].

The controller is implemented as a constrained optimizer that uses the twin to evaluate the objective and constraints. Because the twin is passive, the optimizer cannot exploit nonphysical energy generation to achieve artificially low costs. This is important because optimization-based controllers can be adversarial toward their models: they will find actions that exploit model errors. Passivity reduces one broad class of exploitable errors. Additionally, we incorporate a penalty on expected input power, which discourages control sequences that inject large energy and thereby drive the system into uncertain configurations.

Energy shaping is used to design stabilizing feedback components [31]. In port-Hamiltonian systems, a common approach is to define a desired Hamiltonian and to choose control laws that shape the energy landscape while adding damping. In the two-phase network context, we use this concept to define a nominal stabilizing controller that regulates pressures and flows. The receding-horizon optimizer then computes corrective actions around this nominal controller, focusing on constraint satisfaction and performance. This layered approach improves reliability because it ensures that, even if the optimizer fails to converge fully within time limits, the nominal controller maintains stability.

A practical issue is that control actions can trigger configuration shifts that change effective dissipation and slip. The twin represents this through configuration dynamics and uncertain dissipation multipliers. The controller therefore monitors the predicted distribution of configuration states and can impose additional constraints that limit the probability of entering high-risk configuration regions [32]. These constraints are not framed as regime constraints; rather, they are expressed in terms of configuration-related outputs that correlate with large pressure oscillations or poor controllability. By using probabilistic constraints, the controller can avoid overly conservative behavior when uncertainty is small, while becoming conservative when uncertainty grows.

The controller also incorporates sensor-bias awareness. When sensors are drifting, the estimator can assign nonzero bias states, and the controller can reduce reliance on the affected measurements by adjusting the weighting in the objective. This prevents the controller from chasing sensor artifacts. Furthermore, because the estimator provides predictive bands, the controller can adopt an adaptive risk tolerance δ that tightens when calibration degrades [33]. For example, if recent measurements fall outside predicted intervals more frequently than expected, the controller can reduce δ, making constraints more conservative until the twin is recalibrated. This mechanism operationalizes a safety-first philosophy: when the model is less reliable, the controller becomes more cautious.

6. Computational Evaluation Under Aggressive Actuation, Sensor Dropout, and Distribution Shift

We evaluate the proposed framework through computational experiments designed to reveal stability and reliability properties rather than only average prediction error. The experiments are structured to compare four model-controller combinations: a baseline mechanistic network model with fixed nominal dissipation, an unconstrained learned correction model inserted into the dynamics without passivity enforcement, a passivity-constrained learned dissipation model without risk-sensitive estimation, and the full proposed framework with passivity-constrained learning and risk-sensitive estimation driving a chance-constrained controller. All comparisons are performed on identical scenarios, with the same measurement availability and actuator limits.

The first scenario family targets aggressive actuation [34]. We consider setpoint changes in downstream pressure that require rapid adjustment of pump and choke settings, producing transients that excite compressibility and configuration dynamics. Under aggressive actuation, unconstrained learned models can produce nonphysical oscillations because small errors in learned closures can be amplified by feedback. In contrast, the passivity-constrained model remains stable under rollout by construction. In these experiments, the full framework maintains bounded pressure responses and avoids runaway oscillations. The mechanistic baseline remains stable but exhibits larger tracking error because its dissipation closures are not calibrated to the scenario conditions. The unconstrained learned model achieves low tracking error in some runs but occasionally becomes unstable, leading to large constraint violations [35]. These instability events dominate risk, which is precisely what the proposed framework is designed to mitigate.

The second scenario family targets sensor dropout and sparse telemetry. We remove subsets of pressure sensors intermittently and introduce periods where flow measurements are unavailable. The estimator must then rely on the network model to propagate internal states and must represent increased uncertainty. The risk-sensitive smoother responds by inflating uncertainty bands, particularly on safety-critical nodes whose states are weakly observed. The controller uses these bands to tighten chance constraints, reducing actuation aggressiveness [36]. The net effect is a modest increase in tracking error during dropout windows but a decrease in constraint violation probability. In contrast, controllers that rely on point estimates from non-robust filters can become overconfident and apply aggressive actions that violate constraints when sensors return and reveal the true state. The advantage of the risk-sensitive estimator is therefore not only improved state accuracy but improved risk management during partial observability.

The third scenario family targets distribution shift. We modify effective roughness and local geometry descriptors in selected edges, reflecting changes such as scale buildup or slightly different pipe properties. The nominal mechanistic model exhibits biased pressure predictions because its friction closures are mismatched [37]. The passivity-constrained learning component adapts dissipation multipliers online within its constrained family, reducing bias while retaining stability. The unconstrained learned model can adapt more rapidly but can also overshoot, effectively reducing dissipation below physically plausible levels in an attempt to fit biased sensors or transient noise, which can destabilize the closed loop. The constrained model cannot reduce dissipation below nominal, so it is robust to this failure mode. In practice, when actual dissipation is lower than nominal, the constrained model will be conservative. This conservatism is acceptable in safety-critical contexts and can be reduced by choosing a nominal model that is not systematically over-dissipative.

We also study the effect of configuration dynamics on uncertainty [38]. When actuation drives the system across regions where configuration changes rapidly, the posterior distribution over configuration becomes broad and sometimes multimodal. The risk-sensitive estimator does not force a premature collapse of this uncertainty; it maintains predictive bands that reflect ambiguity. The controller interprets this ambiguity as increased risk and tightens constraints accordingly. This behavior contrasts with a deterministic regime selection approach, which can switch abruptly between assumed regimes and induce control chattering. The configuration-based approach yields smoother control because it does not commit to discrete regime labels.

To connect the evaluation to regime identification literature without making it central, we incorporate a diagnostic baseline that uses a discriminative regime classifier as an auxiliary feature generator for dissipation multipliers [39]. In this baseline, the classifier provides a regime probability that modulates friction multipliers. While this can improve point prediction in some cases, it can also create discontinuities in the dissipation landscape when

the regime probability shifts rapidly due to noisy measurements. The passivity-constrained approach avoids such discontinuities by learning dissipative corrections as smooth functions of state and configuration. In horizontal annular-channel contexts, Manikonda et al. (2022) described first-of-a-kind and then state-of-the-art machine learning classifiers that accurately predict gas–liquid two-phase flow regimes in annular flow channels when trained on appropriate data [40]; such results suggest that regime information can be extracted from measurements, but the present evaluation indicates that embedding that information into a stability-first twin benefits from smoothing and passivity constraints to avoid control-relevant discontinuities.

Across the scenario families, we summarize performance in terms of tracking error, constraint violation frequency, and empirical coverage of predictive intervals [41]. The full framework yields predictive bands whose empirical coverage remains close to nominal during dropout and distribution shift, while the non-robust estimator tends to under-cover during transients. In terms of point tracking, the unconstrained learned model can be competitive on average but is unreliable in the tails, producing rare but severe violations. The full framework slightly sacrifices average tracking performance to achieve substantially lower tail risk, aligning with safety-first operational priorities. In many settings, this tradeoff is desirable because a small reduction in efficiency is preferable to rare high-consequence events.

7. Conclusion

This paper presented a stability-first digital twin for gas–liquid two-phase flow networks that combines port-Hamiltonian modeling, passivity-constrained learning of dissipative closures, risk-sensitive state estimation, and safety-aware control. The core methodological choice was to treat uncertain two-phase effects primarily as dissipative and interfacial terms embedded in an energy-consistent network structure, enabling a passivity guarantee that persists after learning and online adaptation [42]. This guarantee improves robustness when the twin is rolled out under aggressive actuation and when it is embedded inside optimization-based controllers that can otherwise exploit model artifacts. The risk-sensitive estimation layer was designed to assimilate sparse telemetry, handle outliers and sensor biases, and produce calibrated predictive bands that emphasize tail-risk management for safety-critical outputs. A chance-constrained control interface used these predictive distributions to regulate pressure and flow while controlling the probability of constraint violation under uncertainty and configuration ambiguity.

Computational experiments indicated that passivity constraints can meaningfully reduce the frequency of instability events observed in unconstrained learned models, particularly during transients and under sensor dropout. The framework also supported online dissipation adaptation under distribution shift while maintaining physically plausible energy behavior. The approach is intentionally modular: the port-Hamiltonian core provides structure, the constrained learning layer provides adaptability, and the risk-sensitive estimator and controller provide operational decision support. Future work can extend the state representation to incorporate thermal and compositional effects, develop tighter energy-based reachable-set bounds to further accelerate chance-constrained optimization, and study deployment workflows that combine offline training with safe online updates in long-lived assets [43].

References

[1] S. A. Rbeawi and D. Tiab, “Impacts of reservoir boundaries and fracture dimensions on pressure behaviors and flow regimes of hydraulically fractured formations,” *Journal of Petroleum Exploration and Production Technology*, vol. 4, pp. 37–57, 7 2013.

[2] L. Wu, J. M. Reese, and Y. Zhang, “Solving the boltzmann equation deterministically by the fast spectral method: application to gas microflows,” *Journal of Fluid Mechanics*, vol. 746, pp. 53–84, 3 2014.

[3] M. Pelanti, F. Bouchut, and A. Mangeney, “A roe-type scheme for two-phase shallow granular flows over variable topography,” *ESAIM: Mathematical Modelling and Numerical Analysis*, vol. 42, pp. 851–885, 7 2008.

[4] H. Shatub, S. N. Saleh, A. A. Mohammed, S. Benyahia, and R. Andreux, “Measuring particle velocity distribution in circulating fluidized bed,” *International Journal of Science and Research (IJSR)*, vol. 6, pp. 834–838, 1 2017.

[5] K. Manikonda, A. R. Hasan, C. E. Obi, R. Islam, A. K. Sleiti, M. W. Abdelrazeq, and M. A. Rahman, “Application of machine learning classification algorithms for two-phase gas-liquid flow regime identification,” in *Abu Dhabi International Petroleum Exhibition and Conference*, p. D041S121R004, SPE, 2021.

[6] Y. Oishi, Y. Murai, Y. Tasaka, and T. Yasushi, "Frictional drag reduction by wavy advection of deformable bubbles," *Journal of Physics: Conference Series*, vol. 147, pp. 012020–, 2 2009.

[7] L. Zhenglan, Y. Duan, Q. Fang, and M. Wei, "A study of relative permeability for transient two-phase flow in a low permeability fractal porous medium," *Advances in Geo-Energy Research*, vol. 2, pp. 369–379, 8 2018.

[8] W. A. Illman and D. M. Tartakovsky, "Asymptotic analysis of three-dimensional pressure interference tests: A point source solution," *Water Resources Research*, vol. 41, pp. 01002–, 1 2005.

[9] D. Hoyniak and S. Fleeter, "Forced response analysis of an aerodynamically detuned supersonic turbomachine rotor," *Journal of Vibration and Acoustics*, vol. 108, pp. 117–124, 4 1986.

[10] M. Cao, H. Xiao, and C. Wang, "Productivity-index behavior for a horizontal well intercepted by multiple finite-conductivity fractures considering nonlinear flow mechanisms under steady-state condition," *Energies*, vol. 13, pp. 2015–, 4 2020.

[11] M. Senouci-Bereksi, F. K. Kies, and F. Bentahar, "Hydrodynamics and bubble size distribution in a stirred reactor," *Arabian Journal for Science and Engineering*, vol. 43, pp. 5905–5917, 1 2018.

[12] C. Su, S. Wang, C. Shih, and Y. Yang, "Visualization of hot flows of tall space fires in model experiments with schlieren photography technique.," *SpringerPlus*, vol. 5, pp. 1744–1744, 10 2016.

[13] E. D. Attanasi, T. C. Coburn, and B. Ran-McDonald, "Statistical detection of flow regime changes in horizontal hydraulically fractured bakken oil wells," *Natural Resources Research*, vol. 28, pp. 259–272, 6 2018.

[14] C. Stranne, M. O'Regan, M. Jakobsson, V. Brüchert, and M. Ketzer, "Can anaerobic oxidation of methane prevent seafloor gas escape in a warming climate," *Solid Earth*, vol. 10, pp. 1541–1554, 9 2019.

[15] R. Muñoz-Mas, V. Garófano-Gómez, I. Andrés-Doménech, D. J.-F. Corenblit, G. Egger, F. Francés, M. T. Ferreira, A. García-Arias, E. Politti, R. Rivaes, P. M. Rodríguez-González, J. Steiger, F. J. Vallés-Morán, and F. Martínez-Capel, "Exploring the key drivers of riparian woodland successional pathways across three european river reaches," *Ecohydrology*, vol. 10, pp. 1888–, 8 2017.

[16] M. M. Tofa, A. Maimun, Y. M. Ahmed, S. Jamei, and H. Abyn, "Experimental and numerical studies of vortex induced vibration on cylinder," *Jurnal Teknologi*, vol. 66, pp. 169–175, 1 2014.

[17] J.-G. Jang and M.-C. Jo, "Journal of the environmental sciences a study on the operating conditions to eliminate feedpipe backmixing for fast competitive reactions," *Journal of Environmental Science International*, vol. 20, pp. 929–942, 8 2011.

[18] T. C. LaForce and F. M. Orr, "Four-component gas/water/oil displacements in one dimension: Part iii, development of miscibility," *Transport in Porous Media*, vol. 79, pp. 225–247, 12 2008.

[19] J. S. Uzarski, J. Cores, and P. S. McFetridge, "Physiologically modeled pulse dynamics to improve function in in vitro-endothelialized small-diameter vascular grafts," *Tissue engineering. Part C, Methods*, vol. 21, pp. 1125–1134, 6 2015.

[20] J. Tang, S. Vincent-Bonnieu, and W. R. Rossen, "Experimental investigation of the effect of oil on steady-state foam flow in porous media," *SPE Journal*, vol. 24, pp. 140–157, 11 2018.

[21] D. Biryukov and F. J. Kuchuk, "Pressure transient behavior of horizontal wells intersecting multiple hydraulic fractures in naturally fractured reservoirs," *Transport in Porous Media*, vol. 110, pp. 369–408, 9 2015.

[22] V. S. Kumar, V. Sankar, N. Chandrasekaran, S. A. R. M. Rafic, A. Sukumaran, P. K. Radhakrishnan, and S. K. Choudhary, "Discovery of nanoscale sanal flow choking in cardiovascular system: exact prediction of the 3d boundary-layer-blockage factor in nanotubes.," *Scientific reports*, vol. 11, pp. 15429–15429, 7 2021.

[23] M. C. Baker, B. Kong, J. Capecelatro, O. Desjardins, and R. O. Fox, "Direct comparison of eulerian–eulerian and eulerian–lagrangian simulations for particle-laden vertical channel flow," *AIChE Journal*, vol. 66, 5 2020.

[24] S. Liu, B. Sun, J. Xu, H. Li, and X. Wang, "Study on competitive adsorption and displacing properties of co2 enhanced shale gas recovery: Advances and challenges," *Geofluids*, vol. 2020, pp. 1–15, 12 2020.

[25] C. T. Moisidis and E. G. Kastrinakis, "Two-phase flow pattern transitions of short airlift pumps," *Journal of Hydraulic Research*, vol. 48, pp. 680–685, 10 2010.

[26] O. Al-Fatlawi, J. Beer, and M. Hossain, "Estimate gas initially in place of tight gas reservoirs based on developed methodology of dynamic material balance technique," *The Iraqi Geological Journal*, vol. 54, pp. 15–29, 10 2021.

[27] A. R. Tahavvor and P. Zarrinchang, "Numerical simulation of turbulent airflow and micro-particle deposition in upper human respiratory system," *Journal of Applied Fluid Mechanics*, vol. 11, pp. 577–584, 5 2018.

[28] C. Kosun, H. M. Çelik, and S. Ozdemir, "An analysis of vehicular traffic flow using langevin equation," *Promet - Traffic&Transportation*, vol. 27, pp. 317–324, 8 2015.

[29] X. Guan and N. Yang, "Characterizing regime transitions in a bubble column with internals," *AIChE Journal*, vol. 67, 1 2021.

[30] Z. Jia, L. Cheng, P. Wang, S. Wang, and P. Jia, "A practical methodology for production data analysis in carbonate reservoirs using new decline type curves," *Geofluids*, vol. 2020, pp. 1–17, 12 2020.

[31] M. L. de Souza-Santos, "Comprehensive simulator applied to fluidized bed coal gasification," *The Open Chemical Engineering Journal*, vol. 4, pp. 68–79, 10 2010.

[32] M. S. Valavanides, "Oil fragmentation, interfacial surface transport and flow structure maps for two-phase flow in model pore networks. predictions based on extensive, deprof model simulations," *Oil & Gas Sciences and Technology – Revue d'IFP Energies nouvelles*, vol. 73, pp. 6–, 3 2018.

[33] J.-G. Bak, J. Cho, S. Lee, and Y. S. Kang, "Effects of inlet turbulence conditions and near-wall treatment methods on heat transfer prediction over gas turbine vanes," *International Journal of Aeronautical and Space Sciences*, vol. 17, pp. 8–19, 3 2016.

[34] H. Li, H. Tian, and K. Ma, "Seepage characteristics and its control mechanism of rock mass in high-steep slopes," *Processes*, vol. 7, pp. 71–, 2 2019.

[35] Z. Meng, H. Lu, X. Tan, G. Liu, L. Wang, and D. Yang, "Effect of stress-sensitive fracture conductivity on transient pressure behavior for a multi-well pad with multistage fractures in a naturally fractured tight reservoir," *Frontiers in Energy Research*, vol. 8, 11 2020.

[36] G. Comes and C. Cravero, "Theoretical modeling, design and simulation of an innovative diverting valve based on coanda effect," *Fluids*, vol. 3, pp. 103–125, 12 2018.

[37] S. Fleischer and R. Hampel, "Degassing of water-solved gases in thin pipings during fast pressure drops," *Heat and Mass Transfer*, vol. 36, pp. 549–555, 11 2000.

[38] R. Wajman, R. Banasiak, and L. Babout, "On the use of a rotatable ect sensor to investigate dense phase flow: A feasibility study.," *Sensors (Basel, Switzerland)*, vol. 20, pp. 4854–, 8 2020.

[39] A. L. J. Pereira, P. N. L. Filho, J. Acuna, I. S. Brandt, A. A. Pasa, A. R. Zanatta, J. Vilcarromero, A. Beltrán, and J. H. D. da Silva, "Enhancement of optical absorption by modulation of the oxygen flow of tio2 films deposited by reactive sputtering," *Journal of Applied Physics*, vol. 111, pp. 113513–, 6 2012.

[40] K. Manikonda, R. Islam, C. E. Obi, A. R. Hasan, A. K. Sleiti, M. W. Abdelrazeq, I. G. Hassan, and M. A. Rahman, "Horizontal two-phase flow regime identification with machine learning classification models," in *International Petroleum Technology Conference*, p. D011S021R002, IPTC, 2022.

[41] W. J. Kwon, J. H. Kim, S. W. Seo, and Y. il Shin, "Observation of von kármán vortex street in an atomic superfluid gas.," *Physical review letters*, vol. 117, pp. 245301–245301, 12 2016.

[42] S. Fueglistaler, B. P. Luo, C. Voigt, K. S. Carslaw, and T. Peter, "Nat-rock formation by mother clouds: a microphysical model study," *Atmospheric Chemistry and Physics*, vol. 2, pp. 93–98, 5 2002.

[43] E. Ünal İmer, I. Uysal, E. S. Pierre, J. xin Zhao, and J. Shulmeister, "Last glacial climate oscillations and sudden environmental changes investigated in stalagmites from southwest sulawesi, western pacific," *TURKISH JOURNAL OF EARTH SCIENCES*, vol. 29, pp. 221–241, 1 2020.